

Key Residues in δ Opioid Receptor Allostery Explored by the Elastic Network Model and the Complex Network Model Combined with the Perturbation Method

Lei Chen, Weikang Gong, Zhongjie Han, Wenxue Zhou, Shuang Yang, and Chunhua Li*



Cite This: *J. Chem. Inf. Model.* 2022, 62, 6727–6738



Read Online

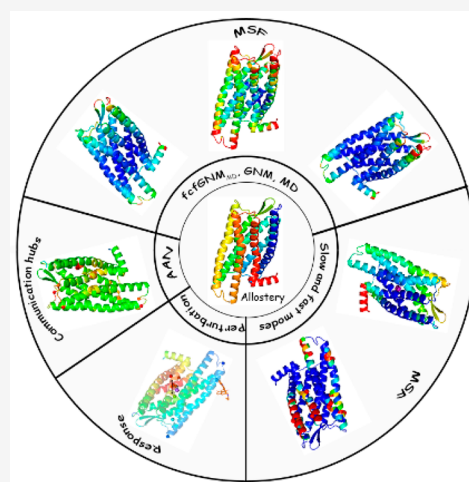
ACCESS |

Metrics & More

Article Recommendations

Supporting Information

ABSTRACT: Opioid receptors, a kind of G protein-coupled receptors (GPCRs), mainly mediate an analgesic response via allosterically transducing the signal of endogenous ligand binding in the extracellular domain to couple to effector proteins in the intracellular domain. The δ opioid receptor (DOP) is associated with emotional control besides pain control, which makes it an attractive therapeutic target. However, its allosteric mechanism and key residues responsible for the structural stability and signal communication are not completely clear. Here we utilize the Gaussian network model (GNM) and amino acid network (AAN) combined with perturbation methods to explore the issues. The constructed $fcfGNM_{MD}$, where the force constants are optimized with the inverse covariance estimation based on the correlated fluctuations from the available DOP molecular dynamics (MD) ensemble, shows a better performance than traditional GNM in reproducing residue fluctuations and cross-correlations and in capturing functionally low-frequency modes. Additionally, $fcfGNM_{MD}$ can consider implicitly the environmental effects to some extent. The lowest mode can well divide DOP segments and identify the two sodium ion (important allosteric regulator) binding coordination shells, and from the fastest modes, the key residues important for structure stabilization are identified. Using $fcfGNM_{MD}$ combined with a dynamic perturbation-response method, we explore the key residues related to the sodium ion binding. Interestingly, we identify not only the key residues in sodium ion binding shells but also the ones far away from the perturbation sites, which are involved in binding with DOP ligands, suggesting the possible long-range allosteric modulation of sodium binding for the ligand binding to DOP. Furthermore, utilizing the weighted AAN combined with attack perturbations, we identify the key residues for allosteric communication. This work helps strengthen the understanding of the allosteric communication mechanism in δ opioid receptor and can provide valuable information for drug design.



INTRODUCTION

G protein-coupled receptors (GPCRs), the largest membrane protein family, mediate signaling pathways involved in many physiological processes such as behavior, cognition, and immune response.¹ Their central role in modulating human physiology makes them key pharmacological targets.² Opioid receptors, a kind of class-A GPCRs, including μ (MOP), δ (DOP), κ (KOP), and orphanin-FQ (OFQ) members³ are associated with pain control. Among them, the DOP is also associated with emotional control, and therefore, the drugs acting on it show additional anxiolytic and antidepressant-like effects.⁴ Thus, the structure and allosteric dynamics of DOP attract extensive attentions.

In 2014, Fenalti et al. crystallized the structure of human DOP in complex with the subtype-selective antagonist naltrindole7 at 1.8 Å resolution.⁵ Similar to other GPCRs, DOP has an extracellular N-terminus, 7 transmembrane (TM) helices (TM1–7), 3 intracellular loops (ICL1–3), 3 extracellular loops (ECL1–3) and an intracellular C-terminus.

The N-terminus and ECLs are responsible for the recognition of a wide variety of ligands, while the C-terminus and ICLs can interact with G protein and GPCR kinase (GRK) effectors, which is essential for signal transduction.⁶ There exist some highly conserved components in TM helices including the D(E)RY motif [Asp145^{3,49}-Arg146^{3,50}-Tyr147^{3,51}] at the bottom of TM3, important for stabilizing the inactive conformation,⁴ the CWxP motif [Cys273^{6,47}-Trp274^{6,48}-Ala275^{6,49}-Pro276^{6,50}] within TM6, usually impairing the activity of GPCR, and the NPxxY motif [Asn314^{7,49}-Pro315^{7,50}-(x)2-Tyr318^{7,53}-(x)6-Phe325^{8,50}] within TM7 important for stabilizing GPCR via forming a conserved polar

Special Issue: Advancing Women in Chemistry

Received: April 29, 2022

Published: September 8, 2022



network.^{7,8} Additionally, experiments have found that sodium ions play a critical role in mediating the allosteric control of GPCRs. The distinctive DOP's sodium ion coordination shells located in a polar network in TM bundle core form two coordination shells, with the first one formed by Asp95^{2,50}, Asn131^{3,35}, Ser135^{3,39}, and two conserved water molecules, and the second one by Trp274^{6,48}, Asn310^{7,45}, Asn314^{7,49}, and two additional water molecules in contact with the waters in the first shell.^{5,9} The sodium ions have a role of stabilizing GPCR in the inhibited state, revealing their important roles in allosteric modulation.⁵

It is difficult for experimental methods to explore the allosteric mechanism in DOP. In 2012, using the X-ray diffraction method, Granier et al. explored the conserved segments involved in opioid ligand recognition, revealing their structural features for ligand subtype selectivity.¹⁰ In 2019, Claff et al. investigated the atomic-scale agonist binding to DOP and identified the key determinants for agonist recognition and selectivity, and receptor activation.⁴ On the theoretical side, Shang et al. used a metadynamics-based strategy to sample the binding process of a positive allosteric modulator BMS-986187 with DOP in the presence of orthosteric ligand SNC-80, revealing two alternative ligand binding poses at the allosteric site delineated by TM1, TM2, TM6, and TM7.¹¹ Utilizing a multiscale simulation strategy, Wang et al. studied the MOP-DOP dimerization and the cooperative mechanism involved in their activation.¹² Additionally, for the important allosteric modulator sodium ions, Yuan et al. simulated their binding process with MOP, indicating that sodium ions enter from the extracellular side and residue Asp95^{2,50} is a possible coordination shell residue.¹³ Similar binding pathways of sodium ions with MOP, KOP, and DOP were observed by Shang et al. using all-atom molecular dynamics (MD) simulations, and they also found that the binding reduces the level of binding of subtype-specific agonists in the three receptors.⁹ Notably, combining long-time scale MD simulations and experiments, Sun et al. explored the allosteric modulation mechanism of sodium ions in DOP, revealing that the sodium ion exploits a distinct conformation of residue Trp274^{6,48} to propagate its modulation to TM5 and TM6, restraining their positions in the intracellular side and inhibiting DOP activation.¹⁴ Currently for the study on allosteric modulation of sodium ions, the mainly adopted scheme is to monitor the ion concentration via MD simulations, and the dynamic responses of DOP molecule system caused by sodium ion binding are not well investigated.

MD simulation is a time-consuming method, especially for large-size systems. Thus, some coarse-grained models have been proposed. Among them, the elastic network model (ENM) is a particularly effective one for investigating the intrinsic dynamics and function-related collective motions in proteins.¹⁵ The Gaussian network model (GNM)^{16–18} and anisotropic network model (ANM)¹⁹ are the two most widely used ENMs. Generally, the low-frequency motion modes obtained by ENM represent the large-scale collective motions relevant to protein functions, while the high-frequency modes reflect the geometric irregularity in protein structure.¹⁷ The ENM model has been successfully used to explore the dynamic characteristics of protein family members,^{20,21} RNA flexibility,^{22,23} RNA/protein folding/unfolding processes^{24,25} and allosteric dynamics of protein-RNA interactions.²⁶ Originally, Tirion et al. proposed the conventional ENM where a protein structure is modeled as an elastic network of C_α atoms in

which the residue pairs within a given cutoff distance are considered to have interactions and are connected by a set of Hookean springs with a uniform force constant.¹⁵ Later, several improved ENMs have been developed including parameter-free ENM (pfENM)²⁷ with the long-range effect of interactions taken into account, RpfGNM method²⁸ based on pfENM with the relative solvent accessibility introduced, sscGNM proposed by us²⁹ with secondary structure considered, and multiscale ENM (mENM) proposed by Xia et al.³⁰ and the modified ewmENM by us³¹ with inter-residue multiscale interactions taken into account. However, there is still much room for the improvement of ENMs. Recently in 2020, Zhang et al. proposed a force constant fitted ENM (fcfENM) where the force constants are directly computed from the inverse covariance matrix using a ridge-type operator for the precision matrix estimation (ROPE) on protein's nuclear magnetic resonance (NMR) ensemble.³² The method obtains an outstanding improvement in residue flexibility reproduction when compared with traditional ENMs. Due to the limited number of NMR data, this method cannot be widely applied. If MD ensemble is available, the method can be applied to a wide variety of biomolecules.

Due to the high effectiveness of ENM, combined with it, some perturbation-response methods have been developed to study protein allostery. In 2009, Atilgan et al. proposed the perturbation-response scanning (PRS) analysis³³ to obtain protein allosteric properties.^{21,34} As the exerted static perturbation force does not allow for the analysis of dynamic effects in allosteric communication, in 2021 Erman et al. developed a dynamic perturbation-response model where a periodic perturbation is exerted based on the solution of the Langevin equation in the presence of solvent, noise and perturbation.³⁵ The method successfully identifies the key residues involved in the allosteric modulation in bovine rhodopsin and nanobody proteins.³⁵

In addition, the complex network model also called amino acid network (AAN) model combined with dynamics methods has been used to study protein allosteric communications.^{36,37} The characteristic path length (CPL) provides an estimation of the effect of node connectivity on communication pathways in a protein. Del Sol et al. found that the residues that greatly affect CPL value upon removal are usually critical to allosteric signal transmission.³⁸ Some studies, including ours, have tried to utilize the attack perturbation to identify the key residues involved in allosteric communication in proteins.³⁹

In this work, we construct a force constant fitted GNM based on MD ensemble (fcfGNM_{MD}) for the δ opioid receptor (DOP). From the lowest and fastest motion modes, we identify the key residues for sodium ion binding and structural stabilization. Utilizing fcfGNM_{MD} combined with the dynamic perturbation-response method, we perturb sodium binding residues and explore the importance of the responding residues. Furthermore, combined with CPL analysis, the AAN with edge weighted by cross-correlation from fcfGNM_{MD} is used to explore the key residues in the allosteric communication.

MATERIALS AND METHODS

Human δ Opioid Receptor and Its MD Ensemble Data. Human δ opioid receptor (DOP) was downloaded from Protein Data Bank (PDB) with PDB ID 4N6H, whose structure is shown in Figure S1. The DOP with 303 residues contains N-terminal region (residues 36–38), TM helices 1–7

(residues 39–77, 82–112, 117–152, 161–187, 205–243, 249–287, and 293–321, respectively), three ICLs (residues 78–81, 153–160, and 244–248), three ECLs (residues 113–116, 188–204, and 288–292), a helical region H8 (residues 322–335), and a C-terminal region (residues 336–338).

The MD simulation trajectories of the structure (ID 73) are available in the GPCRmd database (<http://gpcrmd.org/>),^{40,41} and there are three 500 ns trajectories with IDs 10713, 10714, and 10715. Figure S2 gives the time evolutions of root-mean-square deviation (RMSD) of backbone atoms of DOP during the three simulations. The equilibriums are reached after 220, 100, and 120 ns respectively, and the equilibrium trajectories are used for constructing the fcfGNM_{MD} model of DOP.

Force Constant Fitted GNM Based on the MD Ensemble (fcfGNM_{MD}). Zhang et al. proposed a force constant fitted GNM (fcfGNM) where the force constants are directly calculated from the inverse covariance matrix from NMR ensemble.³² Motivated by the method, we constructed the fcfGNM based on MD ensemble (fcfGNM_{MD}). In fcfGNM_{MD}, the network potential V can be written as follows:

$$V = \frac{1}{2} \sum_{i < j} k_{ij} (R_{ij} - R_{ij}^0)^2 = \frac{1}{2} \sum_{i,j} \Gamma_{ij} \Delta R_i \cdot \Delta R_j \quad (1)$$

Here R_{ij} and R_{ij}^0 are the instantaneous and equilibrium vectors connecting the i th and j th nodes, respectively, k_{ij} is the force constant of the spring connecting the two nodes, the column vectors ΔR_i and ΔR_j represent their fluctuations and the

Kirchhoff matrix $\Gamma_{ij} = \begin{cases} -k_{ij} & \text{if } i \neq j \\ -\sum_{j \neq i} k_{ij} & \text{if } i = j. \end{cases}$ In GNM, the residue

fluctuations are isotropic, and thus the predicted correlated fluctuation between residue i and j is $\langle \Delta R_i \cdot \Delta R_j \rangle = (\Gamma^{-1})_{ij}$, i.e., $C = \Gamma^{-1}$, which is the well-known relationship between covariances and residue–residue interactions. Lezon and Bahar utilized the entropy maximization method⁴² to find the same relationship between covariances and pair interactions: $K = C^{-1}$, where $K = (K_{ij})$ is called the interaction matrix with $K_{ij} = -k_{ij}$ ($i \neq j$) for off-diagonal elements, and covariance matrix C is calculated from the MD ensemble.

The direct computation of the inverse covariance matrix (often called the precision matrix) to obtain the interaction matrix is not appropriate as it is typically a high-dimensional estimation problem. Here, we utilize a ridge-type operator for the precision matrix estimation (ROPE for short).⁴³ The method is of an explicit closed-form representation for the precision matrix as follows:

$$\begin{aligned} F(K, C, \rho) &= \text{tr}(KC) - \log|K| + \rho \|K\|_F \\ C &= UMU^T, M = \text{diag}(m_1, m_2, \dots, m_N) \\ K &= U\Lambda U^T, \Lambda = \text{diag}(\lambda_1, \lambda_2, \dots, \lambda_N) \\ \lambda_i &= 2/(m_i + \sqrt{m_i^2 + 8\rho}), i = 1, 2, \dots, N \end{aligned} \quad (2)$$

where N is the number of residues in the protein, $\|K\|_F = \sum_{ij} K_{ij}^2$ is the Frobenius norm, and $\rho > 0$ is a tuning parameter. The procedure to estimate the interaction matrix K from the covariance matrix C can be simply described as follows: Step 1: Perform eigenvalue decomposition of the covariance matrix C of residue fluctuations and obtain all eigenvalues (m_1, m_2, \dots, m_N) and eigenvectors U . Step 2: Let

$\lambda_i = 2/(m_i + \sqrt{m_i^2 + 8\rho})$, $i = 1, 2, \dots, N$ for a given tuning parameter ρ . Calculate the interaction matrix K according to eq 2. Step 3: Finally, the force constant between residues i and j is estimated as $k_{ij} = -K_{ij}$ ($i \neq j$). It should be pointed out that a reasonable turning parameter ρ needs to be chosen. Here for a given ρ , if the distance of a residue pair (i, j) is larger than a cutoff distance r_c or the calculated force constant of this residue pair is negative, then let $k_{ij} = 0$; otherwise, $k_{ij} = -K_{ij}$. The optimization of the parameters ρ and r_c is described in the following section: **Performance Measures of GNMs.**

The mean square fluctuation (MSF) of the i th node and fluctuation cross-correlation (i.e., correlated fluctuation, CoF) between the i th and j th nodes can be described as $\langle \Delta R_i \cdot \Delta R_i \rangle = (\Gamma^{-1})_{ii}$ and $\langle \Delta R_i \cdot \Delta R_j \rangle = (\Gamma^{-1})_{ij}$. The normalized dynamic cross-correlation between residue fluctuations can be calculated as

$$DCC_{ij} = \frac{\langle \Delta R_i \cdot \Delta R_j \rangle}{[\langle \Delta R_i^2 \rangle \cdot \langle \Delta R_j^2 \rangle]^{1/2}} \quad (3)$$

The values range from -1 to $+1$. The positive values depict that the residues move along the same direction, and the negative ones depict that they move along the opposite directions. The higher the absolute value is, the more the two residues are correlated. The zero value means that the motions of residues are completely uncorrelated.

Performance Measures of GNMs. We use the Pearson's correlation coefficient (PCC) between the theoretical value (x) from GNMs and experimental value (y)⁴⁴ to evaluate the performance of GNMs, which is defined as

$$PCC = \frac{\sum_{i=1}^N (x_i - \bar{x})(y_i - \bar{y})}{\sqrt{\sum_{i=1}^N (x_i - \bar{x})^2 \sum_{i=1}^N (y_i - \bar{y})^2}} \quad (4)$$

where N is the sample size. PCC ranges from -1 to $+1$ with $+1$ representing a perfect positive correlation, 0 no correlation, and -1 a complete anticorrelation.

The optimized parameters are obtained to construct the fcfGNM_{MD} through maximizing the PCC_{AVE} which is defined as

$$PCC_{AVE} = \frac{PCC_{MSF} + PCC_{CoF}}{2} \quad (5)$$

where PCC_{MSF} and PCC_{CoF} indicate the PCC values between the predicted residue MSFs and CoFs by fcfGNM_{MD} and the corresponding values from the MD ensemble, respectively. During the optimization, the tuning parameter ρ and cutoff value r_c are systematically searched in the range of $\{10^{-7}, 10^{-6}, \dots, 10^{-1}\}$ and $\{6 \text{ \AA}, 7 \text{ \AA}, \dots, 15 \text{ \AA}\}$, respectively.

Dynamic Perturbation-Response Method Based on GNM. The dynamic perturbation-response method was proposed by Erman et al.,³⁵ where a residue is perturbed at a given frequency, and the responses of the remaining residues are predicted. The motions of residues in a protein obey the following Langevin equation:

$$M\Delta R' + \zeta\Delta R' + \Gamma\Delta R = F \quad (6)$$

Here ζ is the friction coefficient, F is the external force acting on a chosen residue, ΔR is the residue displacement, Γ is the Kirchhoff matrix from GNM, and M is a diagonal $N \times N$ matrix whose entries equate to the residue masses. Since the masses are several orders of magnitude smaller than friction

forces, the first term is omitted and the equation of motion is as follows:

$$\zeta \Delta R' + \Gamma \Delta R = F \quad (7)$$

We consider a particular force of the form $F = F_p \cos(\omega t)$ acting on the p th residue, with F_p denoting the amplitude of the force. The solution of this equation leads to the residue fluctuation $\Delta R(t)$ as³⁵

$$\Delta R_i(t) = \sum_k F_p \mu_{pk} \mu_{ik} \left[\frac{\lambda_k}{\lambda_k^2 + \zeta^2 \omega^2} \cos(\omega t) + \frac{\zeta \omega}{\lambda_k^2 + \zeta^2 \omega^2} \sin(\omega t) \right] \quad (8)$$

where a time-decay term is omitted on the right-hand side, $\Delta R_i(t)$ refers to the displacement of the i th residue, μ_{pk} and μ_{ik} are the p th and i th components of the eigenvector μ_k , and λ_k is the k th eigenvalue.

The work of the perturbation can be defined as

$$dW = F_p \cdot d\Delta R_p = F_p \cdot \frac{d\Delta R_p}{dt} dt \quad (9)$$

where F_p is the perturbing force vector whose magnitude is $F_p \cos(\omega t)$. In one cycle, the work done is

$$W(\text{one cycle}) = \pi F_p^2 \sum_k \mu_{pk}^2 \frac{\zeta \omega}{\lambda_k^2 + \zeta^2 \omega^2} \quad (10)$$

where the work (denoted as dissipated work) is a function of residue p , frequency, and friction coefficient. The bigger the dissipated work is, the larger the effect the perturbed residue has on the protein. In other words, the dissipated work provides an evaluation of the residues' perturbability, which can be used to identify the probable protein allosteric sites.

Application of a time-dependent perturbation $F = F_p \cos(\omega t)$ on protein residue p generates a perturbation frequency-dependent correlation among residue pairs. If the correlation between the fluctuations of two residues is observed at a time lag of τ , the time-delayed correlation of residue fluctuations will be written as

$$A_{ij}(\omega, \tau) = \langle \Delta R_i(t) \Delta R_j^T(t + \tau) \rangle_t \quad (11)$$

where $A_{ij}(\omega, \tau)$ is the time-delayed correlation of fluctuations between residues i and j , in which the j th residue is observed a time τ after the i th residue is observed. Substituting the displacement given by eq 8 into eq 11, and averaging eq 11 over time t , we obtain

$$A_{ij}(p, \omega, \tau) = A_{ij, \text{sync}}(p, \omega, \tau) + A_{ij, \text{async}}(p, \omega, \tau) \quad (12)$$

where

$$A_{ij, \text{sync}}(p, \omega, \tau) = F_p^2 \sum_k \sum_m \Phi(k, m, \omega) \cos(\omega \tau) \mu_{pk} \mu_{pm} \mu_{ik} \mu_{jm} \quad (13a)$$

$$A_{ij, \text{async}}(p, \omega, \tau) = F_p^2 \sum_k \sum_m \Psi(k, m, \omega) \sin(\omega \tau) \mu_{pk} \mu_{pm} \mu_{ik} \mu_{jm} \quad (13b)$$

in which

$$\Phi(k, m, \omega) = \frac{\lambda_k \lambda_m + \zeta^2 \omega^2}{2(\lambda_k^2 + \zeta^2 \omega^2)(\lambda_m^2 + \zeta^2 \omega^2)} \quad (14)$$

$$\Psi(k, m, \omega) = \frac{(\lambda_k - \lambda_m) \zeta \omega}{2(\lambda_k^2 + \zeta^2 \omega^2)(\lambda_m^2 + \zeta^2 \omega^2)} \quad (15)$$

Equations 13a and 13b show the synchronous and asynchronous components of induced correlations, respectively. The synchronous one $A_{ij, \text{sync}}(p, \omega, \tau)$ (in phase with the perturbation) contains both elastic and dissipative components, and the asynchronous one $A_{ij, \text{async}}(p, \omega, \tau)$ (out of phase with the perturbation) is purely dissipative because it vanishes as friction forces go to zero.

Characteristic Path Length (CPL) Analysis Based on AAN Model. Protein structure and function rely on the complex network of inter-residue interactions.⁴⁵ Here a weighted amino acid model (AAN) is adopted where each residue is represented as a node (C_α atom), and the node pairs within a cutoff distance ($r_c = 13 \text{ \AA}$) are connected by edges which are weighted based on the fluctuation cross-correlation (DCC_{ij}) between residues obtained from fcfGNM_{MD}. The weight w_{ij} of the edge between nodes i and j is calculated as $w_{ij} = -\log(|\text{DCC}_{ij}|)$.

For a network, the characteristic path length (CPL) is defined as the average length of the shortest paths between all pairs of nodes:

$$\text{CPL} = \frac{1}{N_p} \sum_{j>i}^N d_{ij} \quad (16)$$

where N and N_p are the numbers of nodes and node pairs, respectively, and d_{ij} is the shortest path length between nodes i and j . The contribution of a node k to the information communication within a network is measured with the change of the CPL (ΔCPL_k) after removing node k from the network.⁴⁶ A Z -score is used to measure the relative change in CPL:

$$Z\text{-score}_k = \left| \frac{\Delta \text{CPL}_k - \overline{\Delta \text{CPL}_k}}{\sigma} \right| \quad (17)$$

where ΔCPL_k is the change of CPL after removal of node k , $\overline{\Delta \text{CPL}_k}$ is the change ΔCPL_k averaged over all the nodes, and σ is the standard deviation.

RESULTS AND DISCUSSION

Comparison between fcfGNM_{MD} and Traditional GNM. For the structure of DOP, we constructed fcfGNM (denoted as fcfGNM_{MD}) model based on its MD trajectory which can be available from GPCRmd database (<http://gpcrmd.org/>). To estimate reasonably the performance of fcfGNM_{MD}, three DOP fcfGNM_{MD} models were constructed from three equilibrium MD trajectories (MD ensembles) respectively (see Materials and Methods). As a comparison, the three traditional GNM models were also constructed with the cutoff distance optimized with the same method maximizing the average value PCC_{AVE} (eq 5) of the two PCCs (PCC_{MSF} and PCC_{CoF}). Table S1 shows the corresponding results from fcfGNM_{MD} and GNM, as well as the optimized parameters. From Table S1, under the optimized parameters, fcfGNM_{MD} model achieves a PCC_{AVE} value of 0.80 ± 0.04 , much higher than the corresponding value of 0.70 ± 0.03 from the traditional GNM. In the following, we will compare the

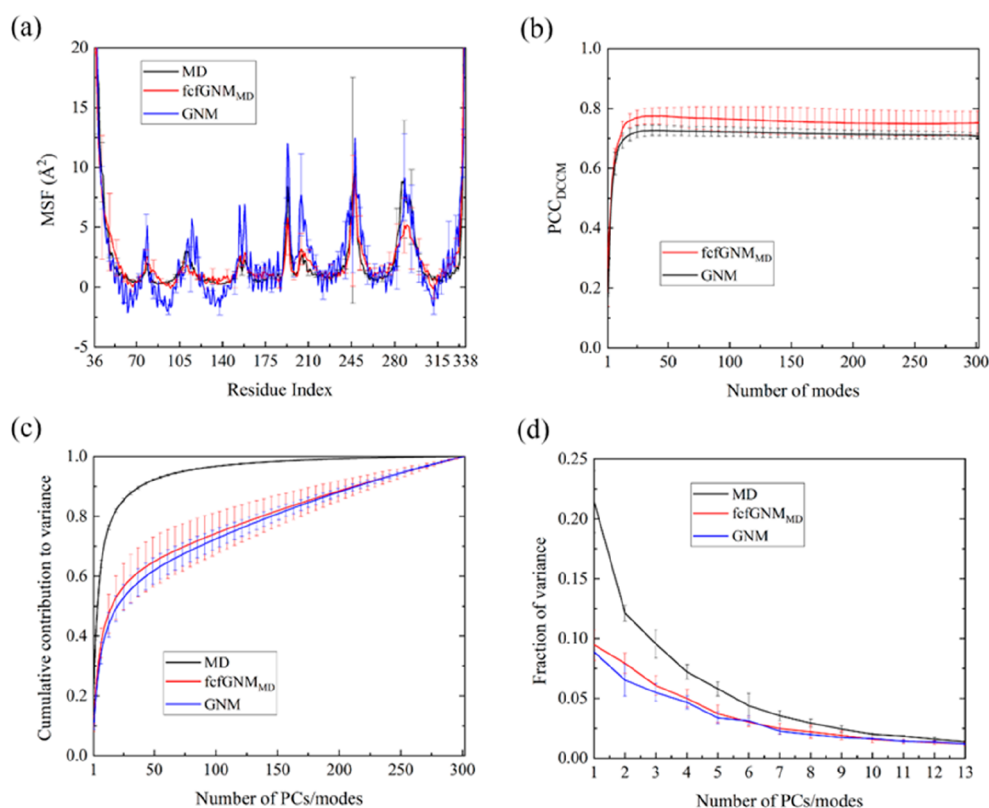


Figure 1. Comparison between $\text{fcfGNM}_{\text{MD}}$ and traditional GNM models constructed based on three MD ensembles. (a) Residue MSF profiles obtained by $\text{fcfGNM}_{\text{MD}}$, traditional GNM and MD ensembles. (b) Change of PCC between DCCMs (PCC_{DCCM}) obtained from MD ensembles and $\text{fcfGNM}_{\text{MD}}$ along with the number of motion modes adopted in $\text{fcfGNM}_{\text{MD}}$, with the corresponding result for the traditional GNM also shown for comparison. (c) Cumulative contributions of PCs/modes from MD ensembles/ $\text{fcfGNM}_{\text{MD}}$ and traditional GNM to the total variance. (d) Fractions of variance captured by the first 13 PCs/modes from MD ensembles/ $\text{fcfGNM}_{\text{MD}}$ and traditional GNM, respectively. The average values and their standard deviations (vertical bar) are shown in each figure.

performances of $\text{fcfGNM}_{\text{MD}}$ and traditional GNM models in terms of reproducing residue MSFs and dynamic cross-correlation maps (DCCMs), as well as capturing motion modes.

Comparison in Reproducing Residue Mean Square Fluctuations (MSFs). The residue mean square fluctuation (MSF) can well describe residue flexibility. Its accurate prediction provides an effective starting point to understand the dynamics of biomolecules. From Table S1, $\text{fcfGNM}_{\text{MD}}$ obtains a PCC_{MSF} value of 0.90 ± 0.03 , much higher than the corresponding value of 0.82 ± 0.02 from the traditional GNM. Figure 1a displays the residue MSF profiles obtained from the two models and MD ensembles, respectively. From Figure 1a, compared with the MSF profile from traditional GNM, the one from $\text{fcfGNM}_{\text{MD}}$ is more like that from the MD ensembles, regardless of the loosely packed segments such as ECLs and ICLs, and the tightly folded regions such as TM helices. We think the main reason lies in that the traditional GNM adopts a uniform force constant, which is insufficient to restrict the loosely packed segments, while exerts an overstrong restriction on the tightly folded regions, resulting in their overhigh and overlow flexibility, respectively. In contrast, the force constants adopted by $\text{fcfGNM}_{\text{MD}}$ are fitted by the inter-residue cross-correlations from MD ensembles, which contributes to the much higher PCC_{MSF} . The $\text{fcfGNM}_{\text{MD}}$ model can consider implicitly the environmental effects to some extent. In addition, the lowest fluctuations lie in the TM regions, while the highest ones appear in ECLs and ICLs, consistent with the

experimental results that TM regions are relatively stable, while ECLs and ICLs are of a relatively high mobility.⁴⁷

Comparison in Reproducing Residue Correlated Fluctuations (CoFs). The residue correlated fluctuation (CoF) can well illuminate the inter-residue motional coupling, helping understand the functional movements of proteins. Table S1 shows that $\text{fcfGNM}_{\text{MD}}$ achieves a PCC_{CoF} value of 0.71 ± 0.05 , significantly higher than the corresponding value of 0.57 ± 0.03 from traditional GNM. The normalized CoFs can be represented as the dynamic cross-correlation map (DCCM). Figure 1b shows the change of PCC between the DCCMs (PCC_{DCCM}) obtained from MD ensembles and $\text{fcfGNM}_{\text{MD}}$ along with the number of motion modes considered in $\text{fcfGNM}_{\text{MD}}$, with the corresponding result for the traditional GNM also shown for comparison. Obviously from Figure 1b, the two curves tend to be steady after a rapid rise, suggesting that a small number of the lowest frequency modes can well describe the motional correlations with the maximum PCC_{DCCM} values of 0.75 ± 0.03 and 0.71 ± 0.02 for the two models. Figure S3 compares the distributions of cross-correlations concerning the inter-residue distance obtained from the two models at the best PCC_{DCCM} values. From Figure S3, for both distribution patterns, the largest positive and negative correlations occur between the residues with the smallest distances apart and half of the maximum distances apart, respectively, consistent with our previous results on six proteins.³¹ The main difference between the two patterns is that quite a few positive correlations are captured by

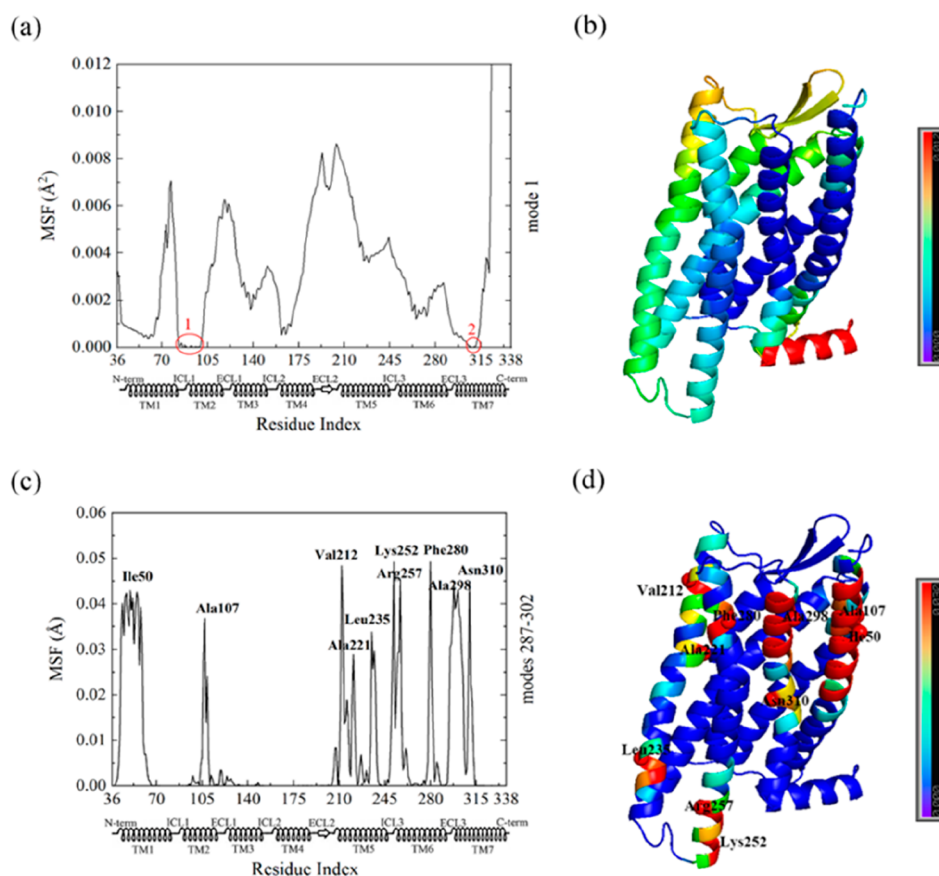


Figure 2. Residue MSF profiles from the slowest mode (a) and from the 16 fastest modes (c) obtained by $\text{fcfGNM}_{\text{MD}}$, with the results mapped on DOP structure shown in parts b and d, respectively. The regions with minimum mobilities in part a are labeled with 1 and 2, and the active residues in part c are shown in the structure in part d. In the color bar on the right, blue and red indicate low and high values of MSF, respectively.

$\text{fcfGNM}_{\text{MD}}$ for the residue pairs beyond half of the maximum distances apart, whose correlations, however, are a little negative in the pattern from the traditional GNM, which implies that $\text{fcfGNM}_{\text{MD}}$ is capable of capturing long-range positive correlations to some extent.

Comparison in Capturing Motion Modes. To evaluate the capability of GNMs in capturing the collective motion modes, we used two indexes: the percentage of the total variance captured by a certain mode (k) $1/\lambda_k/\sum_{i=1}^n 1/\lambda_i$ and the cumulative contribution of the first m modes $\sum_{i=1}^m 1/\lambda_i/\sum_{i=1}^n 1/\lambda_i$, where n is the number of nodes. Figure 1c reports the results for $\text{fcfGNM}_{\text{MD}}$ and traditional GNM, with the corresponding results from MD ensembles obtained by principal component analysis also shown for comparison. From the cumulative contribution (Figure 1c), the curve from $\text{fcfGNM}_{\text{MD}}$ rises faster than that from traditional GNM and is closer to that from the MD ensembles with averagely the first 16 $\text{fcfGNM}_{\text{MD}}$ (21 traditional GNM) modes contributing more than half of the total variance. From the individual contribution (Figure 1d), the ability of $\text{fcfGNM}_{\text{MD}}$ to capture the collective motion modes is better than that of traditional GNM, which can be evidently seen from the contribution rate of the first 2 modes.

To sum up, the above results indicate that $\text{fcfGNM}_{\text{MD}}$ has a more powerful performance in reproducing residue flexibilities and fluctuation cross-correlations, and in capturing the collective motion modes for DOP molecule than the traditional GNM. Thus, we used $\text{fcfGNM}_{\text{MD}}$ to explore the

dynamics of DOP based on the trajectory 10714 (the most stable from Figure S2) in the following study.

Fluctuation Profile from the Lowest-Frequency Mode in DOP.

As we know, the global slow modes represent the large-scale collective motions, which are usually relevant to the functions of biomolecular systems.¹⁷ Previous studies including ours have shown that the most constrained residues in these modes play critical roles, such as hinge and catalytic roles.^{21,48} Adopting the $\text{fcfGNM}_{\text{MD}}$ model constructed based on the MD trajectory 10714, we calculated the residue MSF profile from the first slowest mode of the DOP structure, with the results shown in Figure 2, parts a and b. From Figure 2a, the seven local minimums correspond to TM1–TM7, respectively, and the fluctuation peaks correspond to ECL and ICL regions, implying the DOP regions are well recognized by $\text{fcfGNM}_{\text{MD}}$. Interestingly, we found that there are two regions whose mobilities are constrained severely with fluctuations nearly zero. The first region (residues 83–100) located in TM2 is of certain evolutionary conservation, of which Asp95^{2,50} is a key sodium coordination shell residue, and its mutation has been experimentally found to abolish the “sodium effect”.⁵ The second region (residues 305–311) located in TM7 plays an important role in sodium ion transport, where residues Asn310^{7,45} and Asn311^{7,46} form the second coordination shell of sodium ions.⁵

Fluctuation Profile from High-Frequency Modes in DOP. The fast motion mode corresponds to the irregularity of the local structure of a protein, which is accompanied by a

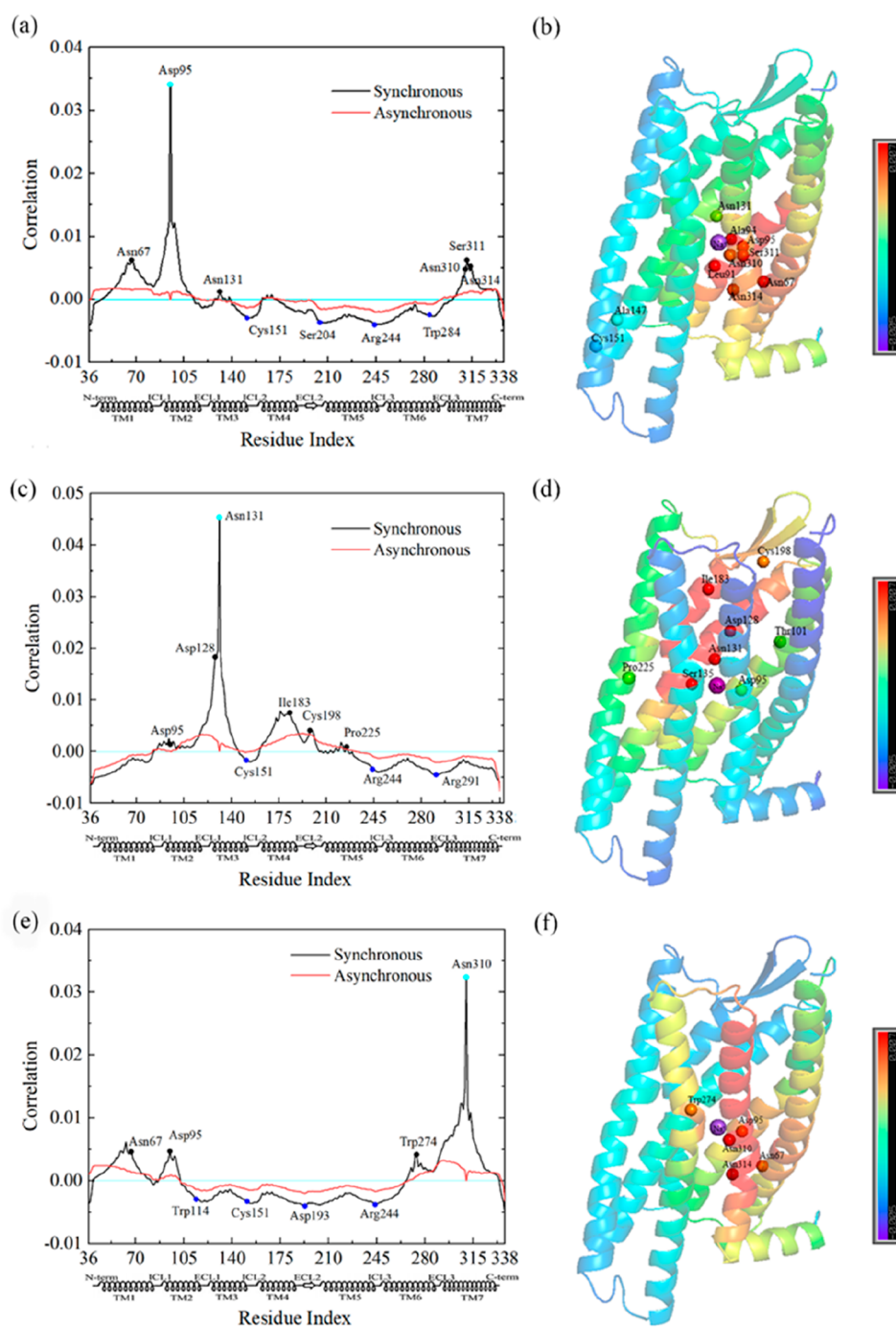


Figure 3. Residue correlations caused by the periodic perturbations on residues Asp95 (a), Asn131 (c), and Asn310 (e), and DOP structures colored by the corresponding synchronous components shown in parts b, d, and f, respectively. The residues evidently coupled to the perturbed residues are highlighted by the spheres colored according to the correlation level with the sodium ion shown as a purple sphere.

large increase in entropy compared with the slow mode.⁴⁹ Previous studies have found that the residues active in the fast mode are generally the hot spots, very important for stabilizing the protein structure.⁵⁰ Parts c and d of Figure 2 show the residue MSFs calculated from the 16 fastest modes of DOP structure. Evidently, the 10 peak centers correspond to Ile50^{1,33}, Ala107^{2,62}, Val212^{5,37}, Ala221^{5,46}, Leu106^{5,60}, Lys252^{6,26}, Arg257^{6,31}, Phe280^{6,54}, Ala298^{7,33}, and Asn310^{7,45}. In the following, we will discuss the functions of the identified key residues based on the available experimental and

theoretical data. The first cluster centered on Ile50^{1,33} includes residues 47–55 (hydrophobic ones except for Thr53) in TM1, which constitute the interface hydrophobic core in I–I dimer of DOP,¹² strengthening the intermolecular interactions. Docking study found that Lys108^{2,63} (in the second cluster) well embedded in a binding pocket forms cation– π and π – σ interactions as a hotspot with BW373U86.⁵¹ Lys214^{5,39} (in the third cluster) located in the hydrophobic pocket lined by Val281^{6,55}, Trp284^{6,58} (both in the eighth cluster), and Leu300^{7,35} (in the ninth cluster) forms cation– π interactions

as a hotspot with a designed ligand (1R, 2R)-6j compound, where the specific packing interactions can well explain why the compound is a selective allosteric ligand to DOP.⁵² Residue Arg257^{6,31} (center of the seventh cluster) forms a hydrogen-bonding network with Leu240^{5,67}, Arg244^{ICL3}, and Val243^{ICL3} and a salt bridge with Asp253^{6,27} (in the sixth cluster), which tethers the intracellular ends of TM5 and TM6, stabilizing DOP in an inactive state.⁵ The pocket residues Phe280^{6,54} (center of the eighth cluster) and Leu300^{7,35} (in the ninth cluster) form multiple hydrophobic contacts with the DPI-287,⁴ contributing a high affinity to the binding. As for the 10th cluster, the center residue Asn310^{7,45} together with Trp274^{6,48} and Asn314^{7,49} construct the second coordination shell of sodium ions in DOP.⁵ Finally, for the fourth and fifth clusters centered on Ala221^{5,46} and Leu235^{5,60} respectively, we have not yet found the reports on their importance for protein stability. They are located at TMS, which displays a large outward movement in the agonist-bound DOP structure,⁴ indicating that they possibly facilitate the stabilization of DOP in an active state.

Furthermore, in order to detect whether fcfGNM_{MD} can consider implicitly the environmental effects to some extent, we performed the similar analyses on DOP complex with naltrindole using fcfGNM_{MD} model constructed based on the complex's 50–400 ns MD trajectory (from GPCRmd database, with time evolution of RMSD of backbone atoms displayed in Figure S4), with the results shown in Figure S5. From Figure S5a, besides the sodium binding pockets, the ligand binding sites (such as Met132^{3,36}, Ile277^{6,51}, and Tyr308^{7,43}) have the most constrained mobilities, and from Figure S5b, several ligand binding residues such as Glu112^{2,67} and Asp293^{7,28} are active in fast modes. These results indicate that the inter-residue interaction differences from MD simulation can be well reflected in the force constants of fcfGNM_{MD}, and fcfGNM_{MD} can consider implicitly the environmental effects to some extent.

Analysis of Dissipated Work Produced by Periodic Perturbations on DOP. A dynamic perturbation-response model based on the traditional GNM was developed by Erman et al. in 2021, where a residue is perturbed periodically and the dynamic responses of other residues are determined.³⁵ In the method, the conception of the dissipated work was proposed, which can be used to evaluate residues' perturbability based on which the probable allosteric sites can be identified. Here, combined the dynamic perturbation with fcfGNM_{MD}, we calculated the dissipated work via eq 10 by perturbing each residue, one by one, with a periodic force with $\xi\omega = \lambda_2$ (the second eigenvalue from fcfGNM_{MD} corresponding to the lowest frequency),³⁵ with the result shown in Figure S6. All the peaks correspond to the loop or turn regions in DOP respectively, implying that perturbing these residues produces a big effect on DOP dynamics. The pronounced peaks correspond to Thr78^{ICL1}, Glu112^{2,67}, Trp114^{ECL1}, Val154^{ICL2}, Asp193^{ECL2}, Ser204^{ECL2}, Arg244^{ICL3}, Gly248^{ICL3}, Ile289^{ECL3}, and Arg291^{ECL3}, respectively. Residue Glu112^{2,67} forms hydrophobic interactions with the allosteric modulator BMS-986187.¹¹ The pocket residues Trp114^{ECL1}, Ile289^{ECL3}, and Arg291^{ECL3} form π - π , hydrophobic, and cation- π interactions with KGCHM07, respectively, stabilizing the activated state of DOP.⁴ Residue Arg244^{ICL3} plays a key role in stabilizing ICL3 by forming an extensive hydrogen-bonding network with other residues from TM6 and TM7, stabilizing DOP in an inactive state.⁵ For other residues, we have not yet found the reports on

their importance for DOP allostery, and they are worthy of further exploration.

Analysis of Dynamic Correlations upon Sodium Ion Coordination Shell Residues Perturbed. The sodium ions have been the study hotspot due to their important allosteric modulation to opioid receptors involved in ligand binding and signal transduction.⁵ The sodium coordination shell residues are similar in some inactive GPCR structures,⁵³ most mutations of which can affect the sodium's allosteric modulation role.¹⁴ To explore the dynamic correlations related to sodium ion binding, we perturbed the sodium ion coordination shell residues including Asp95^{2,50}, Asn131^{3,35}, Asn310^{7,45}, Asn314^{7,49}, and Asp128^{3,32} and calculated other residues' responses based on eqs 13a and 13b, with the results shown in Figure 3 and Figure S7. Among the perturbed sites, the first two and subsequent two are in the first and second coordination shells, respectively,^{5,9} and the last one was found by MD simulation to be the first stop of sodium ions before proceeding to the allosteric sodium coordination shell residue Asp95^{2,50,9}. From Figure 3 and Figure S7, the synchronous and asynchronous components of pair correlations are similar, but the amplitudes are different.

Parts a and b of Figure 3 display the response results when Asp95^{2,50} was perturbed. There are 5 residues Asn67^{1,50}, Asn131^{3,35}, Asn310^{7,45}, Ser311^{7,46}, and Asn314^{7,49} which are coupled positively to Asp95^{2,50}. Asn131^{3,35} is in the first coordination shell of sodium ions, and Asn310^{7,45} and Asn314^{7,49} are in the second one.^{5,9} The highly conserved residue Asn67^{1,50} is a binding hotspot in the I–I dimer of DOP.¹² In addition to the positively correlated residues, residues Cys151^{3,36}, Ser204^{ECL2}, Arg244^{ICL3}, and Trp284^{6,58} show evidently negative correlations with Asp95^{2,50}. These negatively correlated residues are far away from the perturbation point, which shows that perturbation carries information to the far points away from the perturbation point. MD simulation revealed that Cys151^{3,36} is critical for the recognition and interaction of the opioid receptor with fentanyl.⁵⁴ Arg244^{ICL3} stabilizes DOP in the inactive state to some extent.⁵ Trp284^{6,58} forms hydrophobic interactions with SNC-80 and its mutation to Lys affects significantly the ligand binding to DOP.¹¹

Parts c and d of Figure 3 display the response results when Asn131^{3,35} was perturbed. Similar results are obtained when perturbing Asp128^{3,32}, as shown in Figure S7, parts a and b, which is partially because of their adjacency in space. In the following, we only describe the results caused by the perturbation on Asn131^{3,35}. From parts c and d of Figure 3, there are 5 residues Asp95^{2,25}, Asp128^{3,32}, Ile183^{4,60}, Cys198^{ECL2}, and Pro225^{5,50} which are positively coupled to Asn131^{3,35}. Asp95^{2,25} is in the first coordination shell of sodium ions.^{5,9} Asp128^{3,32} is the first stop of sodium ions before proceeding to the sodium coordination shell residue Asp95^{2,50,9}. Cys198^{ECL2} located in a partially hydrophobic pocket participates in the interaction with peptide KGCHM07.⁴ The highly conserved residue Pro225^{5,50} is located in the P–I–F motif, and its inward movement upon DOP activation causes the P–I–F motif's coupling with the rearrangement in the NP^{7,50}xxY motif, which collapses the sodium binding pocket.⁴ In addition, residues Cys151^{3,36}, Arg244^{ICL3}, and Arg291^{ECL3} (far away from the perturbation point) are evidently coupled negatively to Asn131^{3,35}, which are involved in binding with ligands or stabilizing DOP in functional states, as mentioned above.

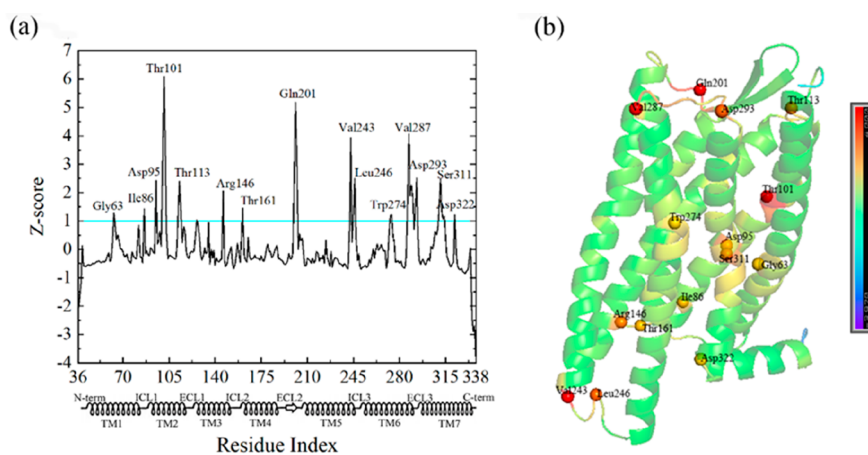


Figure 4. Identified key residues (Z -score >1) by the CPL analysis (a) and DOP structure color-coded by the Z -score value with the key residues highlighted by spheres (b).

Parts e and f of Figure 3 display the corresponding results when Asn310^{7.45} perturbed. Similar results when Asn314^{7.49} (adjacent to Asn310^{7.45}) perturbed are observed, as shown in Figure S7, parts c and d. In the following, we only describe the results caused by the perturbation on Asn310^{7.45}. From parts e and f of Figure 3, there are 3 residues, Asn67^{1.50}, Asp95^{2.50}, and Trp274^{6.48}, which are positively coupled to Asn310^{7.45}. Asn67^{1.50} is a binding hotspot in the I–I dimer of DOP.¹² Asp95^{2.50} and Trp274^{6.48} are in the first and second coordination shells of sodium ions, respectively.^{5,9} Additionally, there are 4 residues, Trp114^{ECL1}, Cys151^{3.55}, Arg244^{ICL3}, and Asp193^{ECL2}, which are coupled negatively to Asn310^{7.45}. The first three are involved in binding with ligands or stabilizing DOP in functional states, as mentioned above.

It should be pointed out that for the above identified residues Asp193^{ECL2}, Ser204^{ECL2}, Ile183^{4.60}, and Ser311^{7.46}, we did not find the experimental data to validate their importance. Since ECL2 is of β -strand fold, typical of all opioid receptor subtypes,⁶ responsible for the recognition of a wide variety of ligands, Asp193^{ECL2} and Ser204^{ECL2} may participate in binding with ligands. Asn310^{7.45} is an allosteric site in the second coordination shell of sodium ions,⁵ which makes us believe its adjacent residue Ser311^{7.46} may play an important role in sodium binding.

From the above analyses, the residue dynamic correlations caused by the perturbations on the sodium ion coordination shell residues suggest that the sodium ion binding is critical to the allosteric modulation to the dimerization of DOP, sodium ion transfer and ligands binding.

Key Residues Identified by CPL Analysis for Allosteric Communication. To identify the key residues of DOP involved in the allosteric communication, we calculated the Z -score of the change in characteristic path length (CPL) when one node is removed from the network, as shown in Figure 4. From Figure 4a, there are 15 key residue clusters that have higher Z -score values (Z -score >1), centered on Gly63^{1.46}, Ile86^{2.41}, Asp95^{2.50}, Thr101^{2.56}, Thr113^{ECL1}, Arg146^{3.50}, Thr161^{4.38}, Gln201^{ECL2}, Val243^{5.68}, Leu246^{ICL3}, Trp274^{6.48}, Val287^{6.61}, Asp293^{7.28}, Ser311^{7.46}, and Asp322^{8.47}, which are mapped on the DOP structure (Figure 4b). According to their positions, the residues can be classified into two groups located at the ECLs/ICLs and adjacent regions and at the TM core region, respectively. In the following, we will discuss the

functions of these residues based on the existing experimental and theoretical data.

For the group of residues located at ECLs/ICLs and adjacent regions, their center residues are Thr113^{ECL1}, Thr161^{4.38}, Gln201^{ECL2}, Val243^{5.68}, Leu246^{ICL3}, Val287^{6.61}, Asp293^{7.28}, and Asp322^{8.47}. Residue Trp114^{ECL1} located in a partially hydrophobic pocket contributes largely to the interactions with KGCHM07.⁴ Thr161^{4.38} is required for the formation of DOP-MOP heterodimers, and Xie et al. found out that the T161^{4.38}A mutant of DOP attenuates morphine antinociceptive tolerance in rats, suggesting Thr161's important role in allosteric signal transmission.⁵⁵ Leu200^{ECL2} located in an active site forms specific interactions with BW373U86.⁵¹ Val243^{5.68} stabilizes ICL3 through an extensive hydrogen bonding network, helping keep DOP in an inactive state.⁵ Leu246^{ICL3} is in the dileucine motif (Leu245^{ICL3}-Leu246^{ICL3}) and Wang et al. found that the deletion of the motif or the mutation of Leu245^{ICL3} slows the lysosomal targeting of the DOP, modifying the receptor trafficking.⁵⁶ Arg291^{ECL3} constrains a distinct loop conformation between TM6 and TM7 through forming hydrogen bonding networks with Val287^{ECL3} and Trp284^{6.58}, which is critical to the selectivity determinant for classical peptide binding to opioid receptors.⁵ MD simulations found Asp293^{ECL3} and Asp288^{ECL3} may be related to the sodium ion binding due to the high sodium densities around the two coordination shells,⁹ and additionally Ile322^{7.39} from MOP plays a key role in the interaction with fentanyl.⁵⁴

For the group of residues located at the TM core region, the cluster center residues are Gly63^{1.46}, Ile86^{2.41}, Asp95^{2.50}, Thr101^{2.56}, Arg146^{3.50}, Trp274^{6.48}, and Ser311^{7.46}. Asp95^{2.50}, Trp274^{6.48}, and Asn310^{7.45} make up the first and second coordination shells of the sodium ion in DOP, respectively, and residue Asp95^{2.50} mutation can abolish the “sodium effect”.⁵ Gly63^{1.46} is an interface residue in the I–I dimer of DOP.¹² Thr101^{2.56} forms specific hydrogen bonds with both Tyr308^{7.43} and Gln105^{2.60}, critical to DOP interaction with DPI-287.⁴ MD simulations found that Asp147^{3.32} establishes a salt bridge with the piperidine nitrogen of fentanyl.⁵⁴ Finally, for the cluster center residue Ile86^{2.41}, we have not yet found the report on its importance for allosteric communications, which needs to be explored in future study.

Based on the analyses above, the key residues identified by the CPL analysis play important roles in DOP's dimerization,

function state stabilization, and interactions with allosteric ligands such as sodium ion, antagonists, and agonists, which are all involved in the allosteric modulation of the DOP.

CONCLUSIONS

Opioid receptors, a kind of G protein-coupled receptors (GPCRs), are the attractive targets for the safe treatment of chronic pain, and in particular, the δ opioid receptor (DOP) has been taken as the molecular targets of anxiolytic and antidepressant due to its additional role in regulating emotional responses. Illuminating the allosteric communication and the key residues involved in DOP's allosteric modulation is critical for understanding the allosteric mechanism and for the associated drug design.

In this work, we construct the Gaussian network model with the force constants from the MD ensemble (fcfGNM_{MD}) and combine it with a dynamic perturbation-response model to explore the dynamics of the DOP and dynamic correlations involved in sodium ion (important allosteric modulator) binding. Additionally, using the weighted amino acid network (AAN) model, we identify the key residues involved in the allosteric communication.

For the fcfGNM_{MD} model, we systemically compare its performance with that of traditional GNM in terms of reproducing residue mean square fluctuation (MSF) and correlated fluctuation (CoF), and capturing functional motion modes. The fcfGNM_{MD} model shows a much better performance in the first two terms with PCC_{MSF} and PCC_{CoF} being 0.90 ± 0.03 and 0.71 ± 0.05 , much higher than the corresponding values 0.82 ± 0.02 and 0.57 ± 0.03 from the traditional GNM. Additionally, compared with the traditional GNM, fcfGNM_{MD} has a more powerful ability to capture collective motion modes and long-range correlations. The improvements are attributed to the fitted force constants in fcfGNM_{MD} based on the MD ensemble.

Next, from the residue fluctuation profile from the slowest mode, the DOP regions including 7 TM helices, 3 ICLs, and 3 ECLs are well recognized. And it is found that the two sodium ion coordination shells have a minimum motility in the DOP structure, which is helpful for the sodium ion binding and further allosteric modulation. Additionally, from the fluctuation profile from the fastest modes, the residues active in the modes are mainly distributed in TMS–7 which play an important role in stabilizing DOP structure or its complex structure with allosteric ligands. Based on the dynamic perturbation-response model, the dissipated work profile obtained through exerting a periodic force on each residue shows that the perturbations on ECL and ICL regions have a larger effect on DOP, and generally, the residues corresponding to the peaks are involved in binding with the allosteric ligands. Additionally, we perform periodic perturbations on sodium ion coordination shell residues to explore the allosteric responses related to the sodium binding. The result reveals that the residues located in the two sodium ion coordination shells have a mutual influence. In addition, the identified other residues with an evident response including Asn67^{1.50}, Trp114^{ECL1}, Cys151^{3.36}, Cys198^{ECL2}, Pro225^{5.50}, Arg244^{ICL3}, Trp284^{6.58}, and Arg291^{ECL3} have been found experimentally or theoretically to participate directly in the DOP's dimerization and binding with ligand or peptides, suggesting that the sodium ion binding allosterically modulates the dimerization of DOP, sodium ion transfer and ligand binding. Interestingly, the key residues negatively coupled with the perturbed residues are far away

from the perturbation points, which are involved in the ligand binding and stabilization of DOP functional states, suggesting the possible long-range allosteric modulation of sodium ion binding for DOP. Finally, by removing one node one time from the weighted dynamic AAN model, we simulate the attack on the network to identify the key residues for allosteric communication. The identified key residue clusters centered on Asp95^{2.50}, Thr101^{2.56}, Thr113^{ECL1}, Arg146^{3.50}, Thr161^{4.38}, Gln201^{ECL2}, Val243^{5.68}, Leu246^{ICL3}, Trp274^{6.48}, Val287^{6.61}, Asp293^{7.28}, Ser311^{7.46}, and Asp322^{8.47}, are vital either for structural stability or for interactions with ligands, which are all related to the allosteric modulation of DOP molecule. Additionally, some identified key residues (such as Ala221^{5.46}, Leu235^{5.60}, Asp193^{ECL2}, Ser204^{ECL2}, Ile183^{4.60}, Ser311^{7.46}, and Ile86^{2.41}) have not yet been verified by experiments. These residues are worthy of further exploration. These identified key residues for binding with allosteric ligands or propagating allosteric signal in this work can be taken as target sites for the design of allosteric effectors (to activate or inactivate DOP molecule) or allosteric modulators (to enhance or weaken the signal propagation).

It should be pointed out that some identified key residues are of high conservation, such as Asn67^{1.50}, Ala107^{2.62}, and Val243^{5.68} important for protein structure stabilization, as well as Thr78^{ICL1}, Ile86^{2.41}, Asp128^{3.32}, and Thr161^{4.38} critical for allosteric signal transmission, which indicates that these highly conserved residue sites probably have individually similar functions in GPCR protein family. In fact, the residue sites Asn^{1.50} and Asp^{3.32} do play an important role in mediating linkage among helices and interactions with ligands in some GPCRs.⁸

As for fcfGNM_{MD}, a kind of ENM methods, although it can consider the effects of membrane, solvent and ion to some extent, and could have a good robustness in the study of protein large-scale collaborative allostery, it still lacks the ability of analyzing specific inter-residue interactions. In the future, the all-atom MD simulations need to be combined with the coarse-grained methods to explore efficiently the allosteric dynamics of opioid receptors. Currently, the structures of δ opioid receptor in different states (active and inactive) have been resolved by X-ray crystallography. We can further study the allosteric characteristics of DOP protein in different states for providing important information to experimental biologists.

ASSOCIATED CONTENT

Supporting Information

The Supporting Information is available free of charge at <https://pubs.acs.org/doi/10.1021/acs.jcim.2c00513>.

Comparison between fcfGNM_{MD} and traditional GNM and the allosteric characteristics of the DOP (PDF)

AUTHOR INFORMATION

Corresponding Author

Chunhua Li – Faculty of Environmental and Life Sciences, Beijing University of Technology, Beijing 100124, China; orcid.org/0000-0002-0895-3506; Email: chunhuali@bjut.edu.cn

Authors

Lei Chen – Faculty of Environmental and Life Sciences, Beijing University of Technology, Beijing 100124, China

Weikang Gong – Faculty of Environmental and Life Sciences, Beijing University of Technology, Beijing 100124, China; orcid.org/0000-0001-8797-784X

Zhongjie Han – Faculty of Environmental and Life Sciences, Beijing University of Technology, Beijing 100124, China; orcid.org/0000-0002-6088-2469

Wenxue Zhou – Faculty of Environmental and Life Sciences, Beijing University of Technology, Beijing 100124, China

Shuang Yang – Faculty of Environmental and Life Sciences, Beijing University of Technology, Beijing 100124, China

Complete contact information is available at: <https://pubs.acs.org/10.1021/acs.jcim.2c00513>

Author Contributions

L.C. and C.L. designed the research. L.C. wrote the program of fcfGNM_{MD} model. L.C., W.G., Z.H., W.Z., and S.Y. performed data analyses. L.C. and C.L. wrote the manuscript. All authors have given approval to the final version of the manuscript.

Notes

The authors declare no competing financial interest.

Data and Software Availability. All data and software used in this manuscript are available. MD simulation trajectory files of DOP are available in GPCRmd: <http://gpcrmd.org/>. The workflow and code of the calculation are available at https://github.com/ChunhuaLiLab/KRE_DOP.

ACKNOWLEDGMENTS

This work was supported by the National Natural Science Foundation of China [32271294, 31971180]. We are committed to supporting and advancing women in chemistry.

REFERENCES

- (1) Conn, P. M.; Ulloa-Aguirre, A.; Ito, J.; Janovick, J. A. G protein-coupled receptor trafficking in health and disease: Lessons learned to prepare for therapeutic mutant rescue in vivo. *Pharmacol. Rev.* **2007**, *59*, 225–250.
- (2) Hauser, A. S.; Attwood, M. M.; Rask-Andersen, M.; Schioth, H. B.; Gloriam, D. E. Trends in GPCR drug discovery: new agents, targets and indications. *Nat. Rev. Drug Discovery* **2017**, *16*, 829–842.
- (3) Pasternak, G. W. Opioids and their receptors: Are we there yet? *Neuropharmacology* **2014**, *76*, 198–203.
- (4) Claff, T.; Yu, J.; Blais, V.; Patel, N.; Stevens, R. C.; et al. Elucidating the active δ -opioid receptor crystal structure with peptide and small-molecule agonists. *Sci. Adv.* **2019**, *5*, No. eaax9115.
- (5) Fenalti, G.; Giguere, P. M.; Katritch, V.; Huang, X.-P.; Thompson, A. A.; Cherezov, V.; Roth, B. L.; Stevens, R. C. Molecular control of δ -opioid receptor signalling. *Nature* **2014**, *506*, 191–196.
- (6) Lee, Y.; Basith, S.; Choi, S. Recent Advances in Structure-Based Drug Design Targeting Class A G Protein-Coupled Receptors Utilizing Crystal Structures and Computational Simulations. *J. Med. Chem.* **2018**, *61*, 1–46.
- (7) Audet, M.; Bouvier, M. Restructuring G-Protein-Coupled Receptor Activation. *Cell* **2012**, *151*, 14–23.
- (8) Angel, T. E.; Chance, M. R.; Palczewski, K. Conserved waters mediate structural and functional activation of family A (rhodopsin-like) G protein-coupled receptors. *Proc. Natl. Acad. Sci. U.S.A.* **2009**, *106*, 8555–60.
- (9) Shang, Y.; LeRouzic, V.; Schneider, S.; Bisignano, P.; Pasternak, G. W.; Filizola, M. Mechanistic Insights into the Allosteric Modulation of Opioid Receptors by Sodium Ions. *J. Biochemistry* **2014**, *53*, 5140–5149.
- (10) Granier, S.; Manglik, A.; Kruse, A. C.; Kobilka, T. S.; Thian, F. S.; Weis, W. I.; Kobilka, B. K. Structure of the delta-opioid receptor bound to naltrindole. *Nature* **2012**, *485*, 400–4.
- (11) Shang, Y.; Yeatman, H. R.; Provasi, D.; Alt, A.; Christopoulos, A.; Canals, M.; Filizola, M. Proposed Mode of Binding and Action of Positive Allosteric Modulators at Opioid Receptors. *ACS Chem. Biol.* **2016**, *11*, 1220–1229.
- (12) Wang, L.; Yuan, Y.; Chen, X.; Chen, J.; Guo, Y.; Li, M.; Li, C.; Pu, X. Probing the cooperative mechanism of the μ - δ opioid receptor heterodimer by multiscale simulation. *Phys. Chem. Chem. Phys.* **2018**, *20*, 29969–29982.
- (13) Yuan, S.; Vogel, H.; Filipek, S. J. A. C. I. E. The Role of Water and Sodium Ions in the Activation of the μ -Opioid Receptor. *Angew. Chem., Int. Ed. Engl.* **2013**, *52*, 10112–10115.
- (14) Sun, X.; Laroche, G.; Wang, X.; Agren, H.; Bowman, G. R.; Giguere, P. M.; Tu, Y. Propagation of the Allosteric Modulation Induced by Sodium in the delta-Opioid Receptor. *Chemistry* **2017**, *23*, 4615–4624.
- (15) Tirion, M. M. Large Amplitude Elastic Motions in Proteins from a Single-Parameter, Atomic Analysis. *Phys. Rev. Lett.* **1996**, *77*, 1905–1908.
- (16) Bahar, I.; Atilgan, A. R.; Erman, B. Direct evaluation of thermal fluctuations in proteins using a single-parameter harmonic potential. *Fold. Des.* **1997**, *2*, 173–181.
- (17) Bahar, I.; Atilgan, A. R.; Demirel, M. C.; Erman, B. Vibrational dynamics of folded proteins: Significance of slow and fast motions in relation to function and stability. *Phys. Rev. Lett.* **1998**, *80*, 2733–2736.
- (18) Bahar, I.; Rader, A. J. Coarse-grained normal mode analysis in structural biology. *Curr. Opin. Struct. Biol.* **2005**, *15*, 586–92.
- (19) Atilgan, A. R.; Durell, S. R.; Jernigan, R. L.; Demirel, M. C.; Keskin, O.; Bahar, I. Anisotropy of fluctuation dynamics of proteins with an elastic network model. *Biophys. J.* **2001**, *80*, 505–515.
- (20) Mikulska-Ruminska, K.; Shrivastava, I.; Krieger, J.; Zhang, S.; Li, H.; Bayir, H.; Wenzel, S. E.; VanDemark, A. P.; Kagan, V. E.; Bahar, I. Characterization of Differential Dynamics, Specificity, and Allostery of Lipoygenase Family Members. *J. Chem. Inf. Model.* **2019**, *59*, 2496–2508.
- (21) Zhang, S.; Gong, W.; Han, Z.; Liu, Y.; Li, C. Insight into Shared Properties and Differential Dynamics and Specificity of Secretory Phospholipase A2 Family Members. *J. Phys. Chem. B* **2021**, *125*, 3353–3363.
- (22) Pinamonti, G.; Bottaro, S.; Micheletti, C.; Bussi, G. Elastic network models for RNA: a comparative assessment with molecular dynamics and SHAPE experiments. *Nucleic. Acids. Res.* **2015**, *43*, 7260–7269.
- (23) Wang, S.; Gong, W.; Deng, X.; Liu, Y.; Li, C. Exploring the dynamics of RNA molecules with multiscale Gaussian network model. *Chem. Phys.* **2020**, *538*, 110820.
- (24) Li, C.; Lv, D.; Zhang, L.; Yang, F.; Wang, C.; Su, J.; Zhang, Y. Approach to the unfolding and folding dynamics of add A-riboswitch upon adenine dissociation using a coarse-grained elastic network model. *J. Chem. Phys.* **2016**, *145*, 014104.
- (25) Su, J. G.; Li, C. H.; Hao, R.; Chen, W. Z.; Xin Wang, C. Protein Unfolding Behavior Studied by Elastic Network Model. *Biophys. J.* **2008**, *94*, 4586–4596.
- (26) Han, Z. J.; Shao, Q.; Gong, W. K.; Wang, S. H.; Su, J. G.; Li, C. H.; Zhang, Y. Interpreting the Dynamics of Binding Interactions of snRNA and U1A Using a Coarse-Grained Model. *Biophys. J.* **2019**, *116*, 1625–1636.
- (27) Yang, L.; Song, G.; Jernigan, R. L. Protein elastic network models and the ranges of cooperativity. *Proc. Natl. Acad. Sci. U.S.A.* **2009**, *106*, 12347–52.
- (28) Zhang, H.; Jiang, T.; Shan, G.; Xu, S.; Song, Y. Gaussian network model can be enhanced by combining solvent accessibility in proteins. *Sci. Rep.* **2017**, *7*, 7486.
- (29) He, J. M.; Han, Z. J.; Farooq, Q. U.; Li, C. H. Study on functional sites in human multidrug resistance protein 1 (hMRP1). *Proteins* **2021**, *89*, 659–670.
- (30) Xia, K. L.; Opron, K.; Wei, G. W. Multiscale Gaussian network model (mGNM) and multiscale anisotropic network model (mANM). *J. Chem. Phys.* **2015**, *143*, 204106.

- (31) Gong, W.; Liu, Y.; Zhao, Y.; Wang, S.; Han, Z.; Li, C. Equally Weighted Multiscale Elastic Network Model and Its Comparison with Traditional and Parameter-Free Models. *J. Chem. Inf. Model.* **2021**, *61*, 921–937.
- (32) Zhang, H.; Shan, G.; Yang, B. Optimized elastic network models with direct characterization of inter-residue cooperativity for protein dynamics. *IEEE/ACM Trans. Comput. Biol. Bioinform.* **2020**, *1*.
- (33) Atilgan, C.; Atilgan, A. R. Perturbation-response scanning reveals ligand entry-exit mechanisms of ferric binding protein. *PLoS Comput. Biol.* **2009**, *5*, No. e1000544.
- (34) Penkler, D.; Sensoy, O.; Atilgan, C.; Tastan Bishop, O. Perturbation-Response Scanning Reveals Key Residues for Allosteric Control in Hsp70. *J. Chem. Inf. Model.* **2017**, *57*, 1359–1374.
- (35) Hacisuleyman, A.; Erkip, A.; Erman, B.; Erman, B. Synchronous and Asynchronous Response in Dynamically Perturbed Proteins. *J. Phys. Chem. B* **2021**, *125*, 729–739.
- (36) Daily, M. D.; Gray, J. J. Allosteric communication occurs via networks of tertiary and quaternary motions in proteins. *PLoS Comput. Biol.* **2009**, *5*, No. e1000293.
- (37) Rader, A. J.; Brown, S. M. Correlating allostery with rigidity. *Mol. Biosyst.* **2011**, *7*, 464–71.
- (38) del Sol, A.; Fujihashi, H.; Amoros, D.; Nussinov, R. Residues crucial for maintaining short paths in network communication mediate signaling in proteins. *Mol. Syst. Biol.* **2006**, *2*, 0019.
- (39) Shao, Q.; Gong, W. K.; Li, C. H. A study on allosteric communication in U1A-srRNA binding interactions: network analysis combined with molecular dynamics data. *Biophys. Chem.* **2020**, *264*, 106393.
- (40) Rodriguez-Espigares, I.; Torrens-Fontanals, M.; Tiemann, J. K. S.; Aranda-Garcia, D.; Ramirez-Anguita, J. M.; Stepniewski, T. M.; Worp, N.; Varela-Rial, A.; Morales-Pastor, A.; Medel-Lacruz, B.; Pandey-Szekeress, G.; Mayol, E.; Giorgino, T.; Carlsson, J.; Deupi, X.; Filipek, S.; Filizola, M.; Gomez-Tamayo, J. C.; Gonzalez, A.; Gutierrez-de-Teran, H.; Jimenez-Roses, M.; Jaspers, W.; Kapla, J.; Khelashvili, G.; Kolb, P.; Latek, D.; Marti-Solano, M.; Matricon, P.; Matsoukas, M. T.; Misztal, P.; Olivella, M.; Perez-Benito, L.; Provasi, D.; Rios, S.; Torrecillas, I. R.; Sallander, J.; Szttyler, A.; Vasile, S.; Weinstein, H.; Zachariae, U.; Hildebrand, P. W.; De Fabritiis, G.; Sanz, F.; Gloriam, D. E.; Cordomi, A.; Guixa-Gonzalez, R.; Selent, J. Publisher Correction: GPCRmd uncovers the dynamics of the 3D-GPCRome (vol 17, 777, 2020). *Nat. Methods.* **2020**, *17*, 861–862.
- (41) Nicoli, A.; Dunkel, A.; Giorgino, T.; de Graaf, C.; Di Pizio, A. Classification Model for the Second Extracellular Loop of Class A GPCRs. *J. Chem. Inf. Model.* **2022**, *62*, 511–522.
- (42) Lezon, T. R.; Bahar, I. Using Entropy Maximization to Understand the Determinants of Structural Dynamics beyond Native Contact Topology. *Plos. Comput. Biol.* **2010**, *6*, No. e1000816.
- (43) Kuismäki, M. O.; Kemppainen, J. T.; Sillanpää, M. J. Precision Matrix Estimation With ROPE. *J. Comput. Graph. Stat.* **2017**, *26*, 682–694.
- (44) Dehouck, Y.; Mikhailov, A. S. Effective Harmonic Potentials: Insights into the Internal Cooperativity and Sequence-Specificity of Protein Dynamics. *Plos. Comput. Biol.* **2013**, *9*, e1003209.
- (45) Di Paola, L.; De Ruvo, M.; Paci, P.; Santoni, D.; Giuliani, A. Protein contact networks: an emerging paradigm in chemistry. *Chem. Rev.* **2013**, *113*, 1598–613.
- (46) Sethi, A.; Eargle, J.; Black, A. A.; Luthey-Schulten, Z. Dynamical networks in tRNA: protein complexes. *Proc. Natl. Acad. Sci. U.S.A.* **2009**, *106*, 6620–6625.
- (47) Fenalti, G.; Zatspein, N. A.; Betti, C.; Giguere, P.; Han, G. W.; Ishchenko, A.; Liu, W.; Guillemin, K.; Zhang, H.; James, D.; Wang, D.; Weierstall, U.; Spence, J. C. H.; Boutet, S.; Messerschmidt, M.; Williams, G. J.; Gati, C.; Yefanov, O. M.; White, T. A.; Oberthuer, D.; Metz, M.; Yoon, C. H.; Barty, A.; Chapman, H. N.; Basu, S.; Coe, J.; Conrad, C. E.; Fromme, R.; Fromme, P.; Tourwe, D.; Schiller, P. W.; Roth, B. L.; Ballet, S.; Katritch, V.; Stevens, R. C.; Cherezov, V. Structural basis for bifunctional peptide recognition at human delta-opioid receptor. *Nat. Struct. Mol. Biol.* **2015**, *22*, 265–268.
- (48) Rader, A.; Chennubhotla, C.; Yang, L.-W.; Bahar, I. The Gaussian Network Model: Theory and Applications. *Normal Mode Analysis.* **2006**, 41–61.
- (49) Li, X. Y.; Zhang, J. C.; Zhu, Y. Y.; Su, J. G. Domain Motions and Functionally-Key Residues of L-Alanine Dehydrogenase Revealed by an Elastic Network Model. *Int. J. Mol. Sci.* **2015**, *16*, 29383–29397.
- (50) Haliloglu, T.; Keskin, O.; Ma, B.; Nussinov, R. How similar are protein folding and protein binding nuclei? Examination of vibrational motions of energy hot spots and conserved residues. *Biophys. J.* **2005**, *88*, 1552–9.
- (51) Pan, C.; Meng, H.; Zhang, S.; Zuo, Z.; Shen, Y.; Wang, L.; Chang, K. J. Homology modeling and 3D-QSAR study of benzhydrylpiperazine delta opioid receptor agonists. *Comput. Biol. Chem.* **2019**, *83*, 107109.
- (52) Shen, Q.; Qian, Y.; Huang, X.; Xu, X.; Li, W.; Liu, J.; Fu, W. Discovery of Potent and Selective Agonists of δ Opioid Receptor by Revisiting the “Message-Address” Concept. *ACS Medicinal Chemistry Letters.* **2016**, *7*, 391–396.
- (53) Huang, W. J.; Manglik, A.; Venkatakrishnan, A. J.; Laeremans, T.; Feinberg, E. N.; Sanborn, A. L.; Kato, H. E.; Livingston, K. E.; Thorsen, T. S.; Kling, R. C.; Granier, S.; Gmeiner, P.; Husbands, S. M.; Traynor, J. R.; Weis, W. I.; Steyaert, J.; Dror, R. O.; Kobilka, B. K. Structural insights into mu-opioid receptor activation. *Nature.* **2015**, *524*, 315–321.
- (54) Eshleman, A. J.; Nagarajan, S.; Wolfrum, K. M.; Reed, J. F.; Nilsen, A.; Torralva, R.; Janowsky, A. Affinity, potency, efficacy, selectivity, and molecular modeling of substituted fentanyl at opioid receptors. *Biochem. Pharmacol.* **2020**, *182*, 114293.
- (55) Xie, W.-Y.; He, Y.; Yang, Y.-R.; Li, Y.-F.; Kang, K.; Xing, B.-M.; Wang, Y. Disruption of Cdk5-associated phosphorylation of residue threonine-161 of the delta-opioid receptor: impaired receptor function and attenuated morphine antinociceptive tolerance. *J. Neurosci.* **2009**, *29*, 3551–3564.
- (56) Wang, W.; Loh, H. H.; Law, P. Y. The intracellular trafficking of opioid receptors directed by carboxyl tail and a di-leucine motif in Neuro2A cells. *J. Biol. Chem.* **2003**, *278*, 36848–36858.